Lab on a Chip

PAPER

View Article Online
View Journal | View Issue

Cite this: *Lab Chip*, 2024, **24**, 5225

A microfluidic hanging droplet as a programmable platform for mammalian egg vitrification†

Haidong Feng ‡§[a] Georgios Katsikis, ‡¶[b] India D. Napier, ‖[c] Gong Du,[c] Josh Lim,[d] Joseph O. Doyle,[d] Scott R. Manalis [abe] and Linda G. Griffith *[a]

Received 17th May 2024,
Accepted 30th September 2024

DOI: 10.1039/d4lc00428k

rsc.li/loc

Egg (oocyte) vitrification is the dominant method for preserving fertility for women of reproductive age. However, the method is typically performed by hand, requiring precise (~0.1 to 10 μL) and time-sensitive (~1 s) liquid exchange of cryoprotectants (CPA) around eggs as well as fine handling of eggs (~100 μm) for immersion into liquid nitrogen (LN_2). Here, we developed a microfluidic platform for programmable vitrification. Our platform is based on a millimeter-sized hanging droplet inside which a given egg is suspended and subjected to liquid exchanges within seconds. After programmable exposures to CPA, the egg is extracted from the liquid–air interface of the droplet using a motorized fine-tip instrument and immersed into LN_2 for vitrification. To benchmark our platform with the manual method, we vitrified over a hundred mouse eggs and found comparable percentages (~95%) for post-vitrification survivability. In addition, our platform performs real-time microscopy of the egg thereby enabling future studies where its morphology may be linked to functional outcomes. Our study contributes to the ongoing efforts to enhance the automation of embryology techniques towards broader applications in reproductive medicine both for clinical and research purposes.

Introduction

Egg vitrification, as a method of rapid freezing,[1] has been established as the dominant method for preserving women's reproductive potential for future use.[2] The removal of the experiment label for vitrification[3] by the American Society of Reproductive Medicine (ASRM) in 2013 caused a boost in the number freezing cycles; in the US alone the annual number of cycles for frozen patient or donor eggs has increased by 400% from 2012 to 2021.[4] However, certain challenges exist for implementing egg vitrification in the clinic. Currently, there is no standard egg treatment protocol, and fertility clinics have various treatment processes, leading to the variation in pregnancy rates utilizing cryopreserved eggs.[2,5] Egg vitrification includes tedious operation steps with requirement of precise control of cryoprotectant dose, timing, and egg handling. The operator's skill has a significant influence on egg survival outcome, and embryologists need multiple years of training to be capable of handling egg freezing.[6,7] Nevertheless, despite the level of training, human error due to fatigue can result in unpredictable outcomes.[8]

Egg freezing is technically challenging due to the large dimension of eggs corresponding to a low surface-to-volume ratio. The egg, with diameter around 150 μm, is the largest cell in the human body, and when frozen, its large size makes it prone to both extra/intracellular ice crystal formation and dehydration, altogether resulting in damage or loss of viability.[9] Egg vitrification[10,11] has become the mainstream approach used in fertility clinics because it addresses these main problems; eggs and the surrounding media transition to an amorphous glassy state without ice crystals. Cryoprotectants (CPA) are used in the vitrification process, which reduces the intracellular water content, and reduces the solution's freezing point. In addition, a rapid cooling process (decrease of ~10 000 °C s^{-1}) is applied by plunging eggs directly into liquid nitrogen while minimizing the media surrounding the egg.

[a] *Department of Biological Engineering, Massachusetts Institute of Technology, Cambridge, Massachusetts 02139, USA. E-mail: griff@mit.edu*
[b] *Koch Institute for Integrative Cancer Research, Massachusetts Institute of Technology, Cambridge, Massachusetts 02139, USA*
[c] *Division of Comparative Medicine, Massachusetts Institute of Technology, Cambridge, Massachusetts 02139, USA*
[d] *Shady Grove Fertility Reproductive Science Center, Rockville, Maryland, 20850, USA*
[e] *Department of Mechanical Engineering, Massachusetts Institute of Technology, Cambridge, Massachusetts 02139, USA*

† Electronic supplementary information (ESI) available. See DOI: https://doi.org/10.1039/d4lc00428k

‡ These authors contributed equally.
§ Present address: Zymeron Corporation, Durham, NC 27709, USA
¶ Present address: Anthology Biotechnologies, Cambridge, MA 02139, USA
‖ Present address: Department of Comparative Pathobiology, Tufts University, N. Grafton, MA, 01536, USA

Egg vitrification results in high egg survival rates after rewarming provided that a delicate treatment process with CPA has been followed before plunging into liquid nitrogen (LN_2) to avoid cryoprotectant toxicity and osmotic stress. As a result, the CPA loading strategy has been carefully studied and nowadays, the standard CPA loading process is traditionally divided into two steps.[12] In the first step, eggs are exposed to a low concentration CPA, namely equilibration solution (ES). ES is gradually loaded, and eggs first dehydrate, losing a small fraction of their volume, and then equilibrate, slowly recovering some of the volume loss. This step traditionally lasts for 10–15 minutes. In the second step, eggs are exposed to a high concentration CPA, namely vitrification solution (VS). As opposed to ES, VS is quickly loaded; the long-term exposure to VS is toxic to eggs, and eggs need to be vitrified in liquid nitrogen within a short time (60–90 s) after VS loading. After exposure to VS, eggs are plunged into liquid nitrogen *via* a vitrification carrier, where they will be held for long-term storage. Open and closed vitrification carrier systems, such as open pulled straw, CryoTop, capillary tube, Rapid-I, and Cryoloop,[13–16] have been developed. To maintain high cooling rates and avoid intracellular ice crystal growth, it is deemed important to minimize VS volume (<0.1 μL) around the egg on the vitrification carrier.

Microfluidic systems have been widely used in the field of assisted reproductive technology (ART) for gametes sample preparation and *in vitro* diagnostic processes.[17–20] In the context of vitrification, systems are either closed or open depending on where the eggs are handled. In closed systems, eggs are handled inside microfluidic channels. CPA loading is gradually done utilizing the diffusion of CPA inside the microfluidic channels.[21–24] The local environment, such as CPA concentration and temperature, has also been controlled to study egg response during CPA loading.[25] However, certain challenges exist related to manual processes for loading or unloading eggs in closed systems. These processes increase operation complexity, and may physically damage the eggs or cause their loss due cell trapping and air bubbles in the system. In open systems, eggs are handled in air–liquid interfaces, such as wells or droplets.[26–30] CPA loading is done by dispensing CPA over eggs located in microfluidic traps at the bottom of wells,[26,27] mixing droplets with different CPA concentrations[28] or injecting CPA using microfluidic needles in contact with droplets containing eggs.[29] These open systems, allow for easier egg loading and unloading processes than in closed systems and have so far led to multiple commercialization efforts. For example, Genea Biomedx proposed *Gavi* for semi-automated embryo and egg vitrification process.[27,31,32] *Gavi* used chips that not only load the CPA but also serve as vitrification carriers without need for egg relocation, however they have low cooling rates, thus compromised egg survival rates compared to traditional vitrification carriers.[14] Overture launched *DaVitri* system for programmed cryoprotectant loading,[33] however after exposure to CPA, *DaVitri* requires skill to reliably unload eggs with a fine tip instrument by hand before plunging into liquid nitrogen. Notably, in all these systems, eggs are in contact with solid walls while in microfluidic traps[26,27] or at the bottom of standing droplets, often limiting the speed of liquid exchange or requiring multiple steps for unloading eggs from droplets.[29,30]

In this paper, we propose a programmable microfluidic system for egg vitrification. Our microfluidic system includes a disposable microfluidic chip featuring a hanging droplet inside which a given egg is suspended and subjected to liquid exchanges within seconds. After programmable exposures to CPA, the egg is extracted from the liquid–air interface of the droplet using a motorized fine-tip instrument and immersed into LN_2 for vitrification. The contactless egg handling approach minimizes physical damage and egg loss. Our platform is user-friendly and provides consistent outcomes with real-time monitoring of the overall process.

Platform development

Design of microfluidic chip

We based our platform on a microfluidic chip that forms a hanging droplet where eggs undergo liquid exchanges according to vitrification protocols (Fig. 1). In particular, our chip includes three inlets for flowing basic (BS), equilibration (ES) and vitrification (VS) solutions and one waste (W) outlet (Fig. 1a). We constructed the chip (Fig. 1b) from cyclic olefin copolymer (COC, Topas) which exhibits chemical resistivity to cryoprotectant components such as dimethyl sulfoxide (DMSO), and is bio-compatible due to its solvent-free fabrication process (Materials and methods). We fabricated the chip as a multilayer design featuring microfluidic channels and cover layers patterned on thin (250 μm) COC sheets using a vinyl cutter (GS2-24, Roland), and then bonded the components through thermal lamination[34,35] (Fig. 1c and S1†). The microfluidic chip includes multiple layer flow channels that get interconnected and form an orifice at the tip of the microfluidic chip; when liquids flow into the orifice, a hanging droplet forms (Fig. 1d). To prevent liquid spreading from the orifice, we incorporated a rim of COC produced using CNC milling (Bantam Tools), then thermally bonded to the main chip using a COC elastomer (E140, Topas) as an adhesive layer[34] (Fig. S1†).

Scaling properties for the microfluidic chip

The hanging droplet serves as a stable chamber for exposing eggs to liquid exchanges (Fig. 1e). To ensure droplet stability against the influence of gravity, we designed the system to a millimeter-length scale L as dictated by the Bond number $B_o = \rho g L^2/\sigma$, expressing the ratio of gravitational over surface tension forces. Setting $B_o = 1$ and characterizing the densities ρ and surface tension σ of our liquids using a goniometer (Model 590, Rame-Hart), we calculated $L \approx 2$ mm. Above the hanging droplet, there is an additional liquid–air interface that serves as an entry point for loading the egg into the chip (Fig. 1e). Given a typical size ($d \approx 100$ μm) and density ($\rho_e \approx$

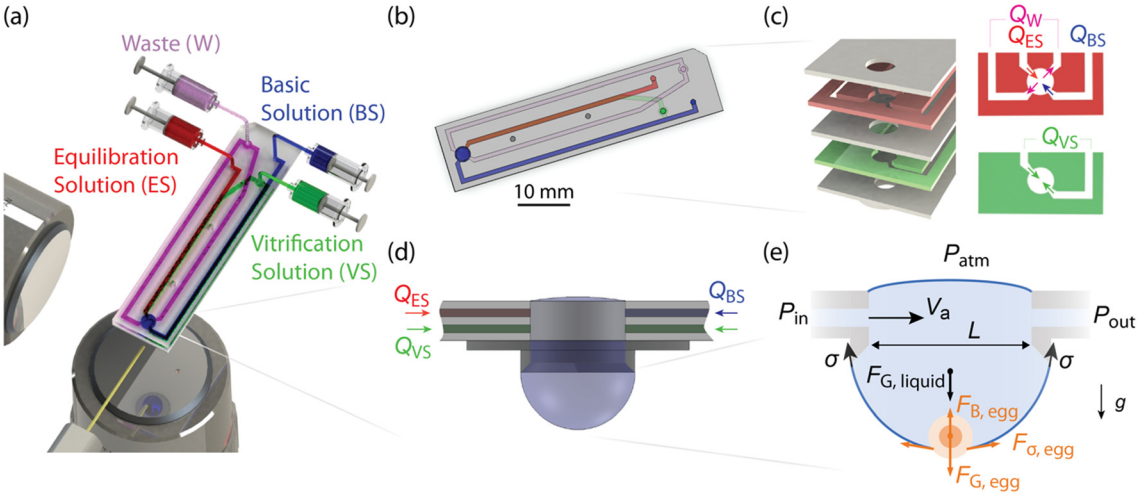

Fig. 1 Structure and operating principle of microfluidic chip for egg vitrification. a) Schematic (syringes not in scale) of microfluidic chip with 3 inlets (BS, ES, VS) and an outlet (W). The operation is monitored using two microscope objectives (Materials and methods). b) Drawing of chip c) break-view of design of chip (left) with color coding denoting distinct layers (right) featuring the inlets and outlets, where Q denotes flows with same notation as in (a). d) Profile view at the tip of chip where a hanging droplet is formed from flow of liquids. e) Simplified schematic (showing a single inlet) featuring an open surface on top (P_{atm} is atmospheric pressure), of a hanging droplet of liquid hosting an egg (orange) at its bottom *via* interfacial tension. F_G denotes weight, F_B buoyancy and, F_σ interface tension forces. L denotes length scale of droplet, V_a denotes advection velocity $V_a = Q/A$ where A is area of inlet and g is gravitational acceleration and σ interfacial tension. Due to inlet and outlet flows, $P_{in} > P_{atm}$ and $P_{out} < P_{atm}$.

1100 kg m^{-3}) of a mammalian egg, we estimated the sedimentation time-scale $\tau_s = L/V_s$, where the sedimentation velocity $V_s = (\rho_e - \rho)d^2g/18\mu$, where μ is the dynamic viscosity of liquid and g acceleration of gravity. Based on fluid properties (Table 1), we estimated $V_s = 0.5$ mm s^{-1}, hence a time-scale $\tau_s \approx 4$ s for facile sedimentation of the egg from the open liquid-interface at the top of the chip to the tip of the hanging droplet (Fig. 1e). Once the egg reaches the tip of the droplet, it is held by interfacial tension forces at the liquid–air interface. The replacement of liquid air interface with egg surface causes a trapping energy to minimize surface area. The induced capillary force supports the egg from buoyancy while preventing it from moving around.

To estimate the required flow rate Q to exchange liquids around an egg inside the hanging droplet, we set a desired liquid exchange time scale $\tau_e \approx 1$ s consistently with vitrification protocols. Given that the diffusivities[36] of main components (DMSO, sucrose) of CPAs into water are $D \approx 10^{-9}$ m s^{-1}, we calculated a diffusion time scale $\tau_D = L^2/D \approx 1$ h. Given that $\tau_D \gg \tau_e$, advection is required for adequate liquid exchange. We thus set an advection time scale $\tau_a = \tau_e/10 \approx 0.1$ s, given that the incoming cryoprotectants into the hanging drop do not have plug flow characteristics. We formulated $\tau_a = L/V_a$, where $V_a = Q/A$ is the characteristic flow velocity (Fig. 1e) at an inlet of cross-section area $A = tw \approx 1.25 \times 10^5$ μm^2 (set by thickness $t = 250$ μm of COC sheets and $w = 500$ μm per resolution of vinyl cutter), thus calculating $Q \approx 150$ μL min^{-1} and an intermediate Reynolds number $Re = \rho V_a L/\mu \approx 50$ for the flow regime.

Development of integrated platform

Based on our microfluidic chip design, we developed an integrated platform that performs vitrification in three steps: egg loading, visually-monitored CPA loading, and egg unloading (Fig. 2 and S2†).

First, the egg is pipetted into the air–liquid interface on the top of the chip and allowed to sediment at the bottom tip of the hanging droplet (Fig. 2a). Second, the egg is sequentially exposed to cryoprotectants consisting of equilibration solution (ES) followed by vitrification solution (VS) with an interval in between ES and VS. We load these cryoprotectants by

Table 1 Cryoprotectant composition and fluid properties

Name	Composition	Density ρ (g cm^{-3})	Viscosity μ (Pa s)	Surface tension σ (dyns cm^{-1})
Basic solution (BS)	Human tubal fluid (HTF) + 20% human serum albumin (HSA)	0.983	9.75×10^{-4}	46.91
Equilibration solution (ES)	BS + 7.5% DMSO + 7.5% EG	0.988	1.48×10^{-3}	45.36
Vitrification solution (VS)	BS + 15% DMSO + 15% EG + 0.5 M sucrose	1.095	3.93×10^{-3}	44.76
Thawing solution (TS)	BS + 1.0 M sucrose	1.136	5.5×10^{-3}	69.86
Dilute solution (DS)	BS + 0.5 M sucrose	1.067	1.63×10^{-3}	52.66

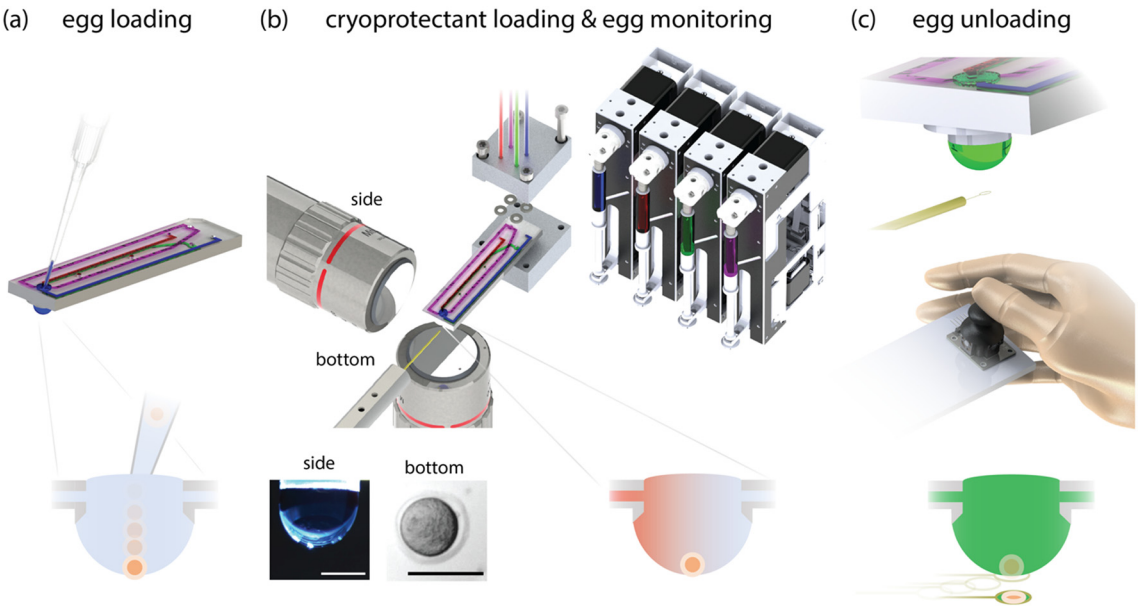

Fig. 2 Integrated platform for performing vitrification in three steps. a) The egg is loaded *via* pipetting (top, only pipette tip is shown) on the microfluidic chip from open orifice at the top side of hanging droplet (bottom). b) Cryoprotectants (ES, VS) are sequentially loaded on hanging droplet, where assembly is shown in break-down view featuring tubing, custom-machined clamp, O-rings and two microscope objectives for obtaining side and bottom view of hanging droplet *via* CMOS cameras (not shown). The bottom view allows for monitoring the egg in real-time. The flows are delivered using syringe pumps (Materials and methods). Scale bars are 2 mm (side view) and 100 μm (bottom view) c) The egg is loaded into the tip of the hanging droplet (top) using a Cryoloop, a vitrification carrier in the form of a thin Nylon wire (Fig. S4c and Video S2†) that we control using a custom-made micromanipulator (middle, Fig. S4b and Video S1†). The egg is unloaded when the Cryoloop touches the tip of the hanging droplet (Fig. S4d†).

programming syringe pumps (Hamilton PSD6/SF, NV, USA) that deliver the ES and VS flows using a custom-designed aluminum cartridge, which contains inlet and outlet ports that are tightly coupled to the microfluidic chip (Fig. 2b). The process of cryoprotectant loading is monitored in real-time using two microscope objectives placed in an orthogonal arrangement. The horizontal objective (Mitutoyo compact 1X objective, 375-036-2) is coupled to a color camera (Allied Vision, 1800 U-1242), and obtains a side view of the droplet (Fig. 2b, side and S2b†), enabling us real-time calculation of its volume (Materials and methods). The vertical objective (infinity-corrected, long working distance Nikon 4X, MRH00045) is coupled to a monochrome camera (Basler, a2A4504-18umPRO) and obtains the bottom view of the droplet focused at its tip where the egg is located (Fig. 2b and S2b†). We mounted the vertical objective on a motorized stage (Thorlabs MT1-Z9, KDC101) to maintain the focus on the egg whenever there were small variations on the height of the hanging droplet given the narrow depth of field DOF ≈ 2 μm for our objective (numerical aperture of NA = 0.13). To resolve the morphology of the egg in real-time during cryoprotectant loading, we not only selected a camera with suitable (2.58 μm) optical resolution, but also designed an illumination system with non-collimated light given the convex shape of the droplet (Materials and methods).

Third, the egg is unloaded from the chip after exposure to VS using Cryoloop,[37] a closed-loop thin (≈20 μm diameter) Nylon wire (Fig. 2c, S3 and S4c†). Previous studies with human eggs using Cryoloop as a vitrification carrier showed high vitrification recovery and survival rates.[37–39] To remove the need for manual handling of the Cryoloop during unloading of the egg from the chip, we attached the Cryoloop to a motorized 3-axis translation stage (Thor Labs, LTS150C) *via* a custom-designed 3d-printed holder. We actuated the 3-axis stage with a joystick system (SMAKN Fr4 Ky-023) and a microcontroller (Arduino Uno) to control the position of the Cryoloop (Fig. S4b and c†). When a dry Cryoloop touches the liquid–air interface, interfacial tension draws a thin film of cryoprotectant containing the egg to the Nylon wire (Fig. 2c, S4d and Video S1†). Due to the high hydrophilicity of Nylon, the liquid film is thin, as remains confined within the thickness (≈20 μm diameter) of the wire (Fig. S4d and Video S2†). The egg can then be plunged into a liquid nitrogen tank for vitrification. The entire vitrification process (including liquid handling, imaging, to Cryoloop control and data acquisition) is centrally controlled using a custom program (LabVIEW 2020, Materials and methods).

Results and analysis

Simulation of liquid exchange inside the hanging droplet

To gain insight into the liquid exchange inside the hanging droplet, we performed computational fluid dynamics simulations using commercial software (COMSOL 6.1). We assumed a steady liquid–air interface with slip boundary condition (Materials and methods) and a typical droplet volume of V_d = 20 μL which is stable in our system ($B_o \approx 1$).

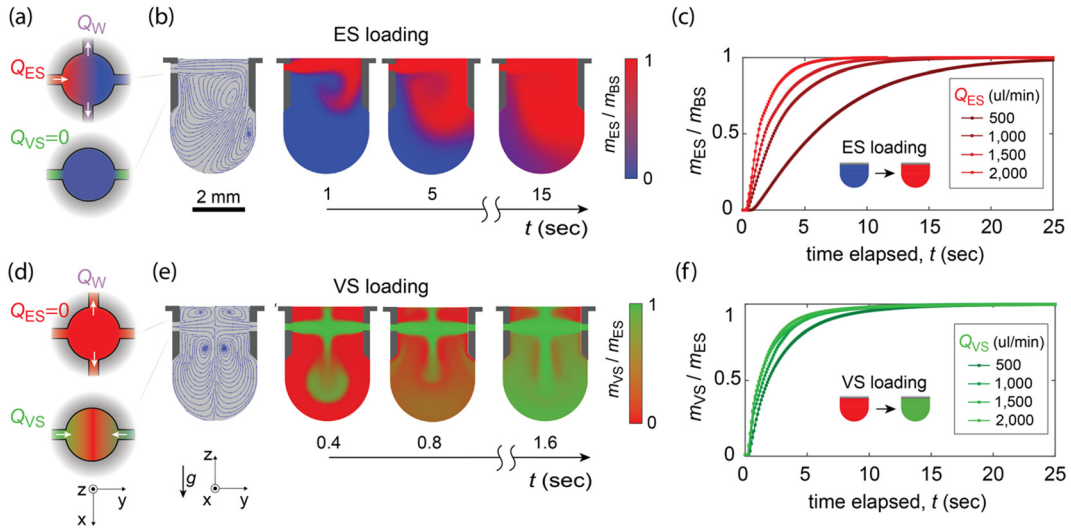

Fig. 3 Simulation of flow patterns and liquid exchange inside the hanging droplet. a) Schematic of top-view cross-sections of chip during ES loading. b) COMSOL simulation results of side-view streamlines (left) and color maps showing local mass ratio m_{ES}/m_{BS} at Q_{ES} = 500 μL min^{-1}. c) Mass ratios averaged over droplet volume exposed to atmosphere (inset) showing liquid exchange for various flow rates for ES derived by COMSOL simulations (Materials and methods). d–f) Equivalent graphs to a–c for VS loading at Q_{ES} = 1500 μL min^{-1}.

Under these assumptions, we studied loading of CPAs in two steps: ES loading for exchanging BS with ES, and VS loading for exchanging ES with VS (Fig. 3).

We used our simulations to predict the time scale for liquid exchange in each loading step. In ES loading, ES enters the hanging droplet through a single inlet while waste solution exits through a double outlet (Fig. 3a). We observed that the resulting flow pattern is asymmetric across the midplane of the droplet, and ES gradually displaces the BS (Fig. 3b, plane *zy*). Moreover, we quantified ES loading as the mass ratio of ES over BS averaged over the volume of the hanging droplet, and found that liquid exchange occurs within 5–20 s depending on the flow rate (Q_{ES} = 500–2000 μL min^{-1}) (Fig. 3c). In VS loading, VS enters the hanging droplet through a double inlet (Fig. 3d), and the resulting flow pattern is symmetric across the midplane of droplet (Fig. 3e, plane *zy*). In our system, fluid properties such as viscosity, density (Table 1) as well as the characteristic length L and velocity V_a (which is affected if there is a single or double inlet) altogether determine the interplay between inertial, viscous and gravitational (or buoyant) forces resulting in a time scale for loading liquids (liquid exchange). By invoking the dimensionless Reynolds *Re* and Archimedes *Ar* numbers, we observed that VS loading occurs at a regime of lower inertial/viscous (*Re*) forces and higher buoyancy/viscous (*Ar*) forces than those for ES, generally resulting in shorter times τ ($\tau_{VS} < \tau_{ES}$) for liquid exchange (Fig. S5†). On one hand, at lower flow rates (*e.g.* Q = 500 μL min^{-1} or $Re < 150$) VS loading (Fig. 3f) occurs much faster ($\tau_{VS} \ll \tau_{ES}$) than ES loading (Fig. 3c), due to buoyancy forces determining liquid exchange. On the other hand, at higher flow rates (*e.g.* Q = 1500–2000 μL min^{-1} or $Re > 150$), VS and ES loadings occur at similar time scales (τ_{VS}, τ_{ES} around 5–10 s) due to inertial forces or advection having a greater role determining liquid exchange than for that for lower flow rates.

Experimental characterization of liquid exchange inside the hanging droplet

To experimentally validate the time scales of liquid exchange from our simulations, we used our syringe pumps to load ES and VS into the hanging droplet (Fig. 2b). For the purpose of characterization, we used distinct food dyes (1 drop per 10 mL) for each one of BS, ES, VS solutions (Shady Grove Fertility), enabling us a direct visual cue for each type of liquid present in the hanging droplet. Therefore, we sequentially flowed ES and VS solutions into the chip for same flow rates (Q = 500–2000 μL min^{-1}) as in simulations (Fig. 4, S6 and Video S3†). Synchronizing the dispensing syringe (ES or VS) with the aspirating syringe (W) at any given time, we attained the desired flow rates (Fig. 4a and S6†) while maintaining a practically constant droplet volume during operation (Fig. 4b and S6†). In particular, we calculated the droplet volume in real-time by using our microscopy system (Fig. 2b, side) and a brightness-thresholding algorithm (Fig. S7,† Materials and methods), and found that the variation of droplet volume was below 5% during ES and VS loading (Fig. 4b and S6†). Simultaneously, we quantified in real-time the RGB (red–blue–green) color ratios of the hanging droplet (Fig. 4c and S6†). In that manner, we obtained a direct visual cue of "cascade" color change of the droplet as BS (blue) was exchanged with ES (red) and finally with VS (green) (Fig. 4d and S6†). The molar concentration of food dyes in our solution are low (≤1 mM), and we assumed that they had a negligible effect on fluid properties with regards to the time scales of liquid exchange (ESI†). We used the color change as a quantitative proxy for liquid exchange. Specifically, we used the R/B (ES/BS) and G/R (VS/ES) ratio curves for respectively

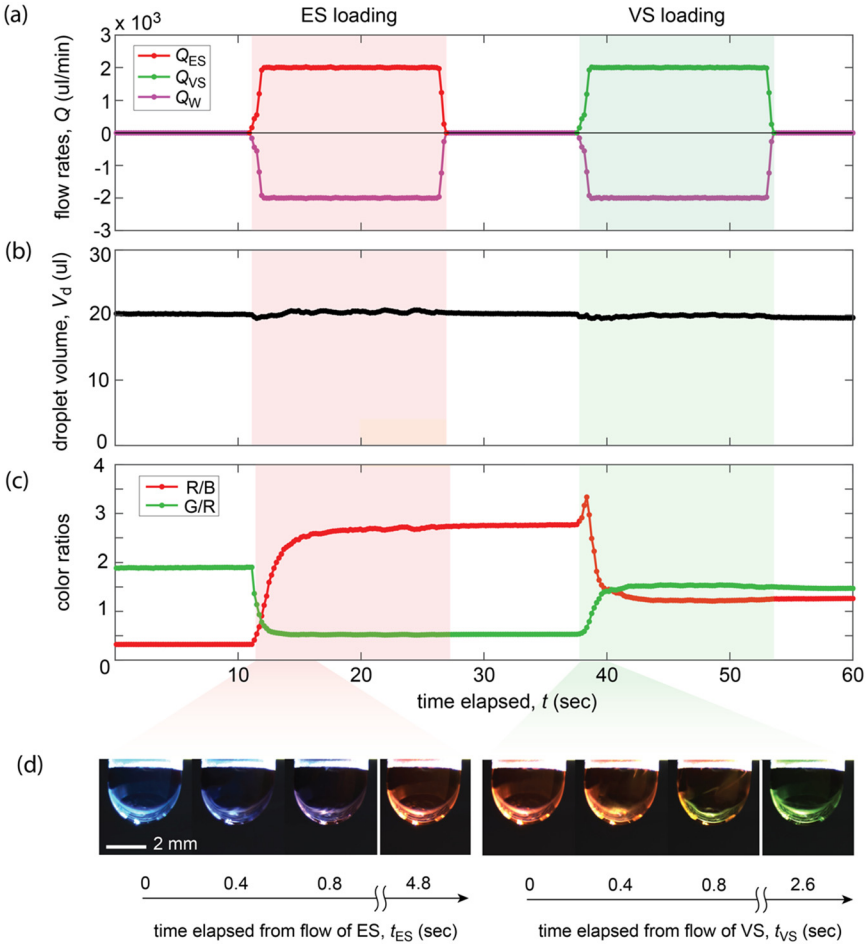

Fig. 4 Experimental characterization of flow control, droplet stability and liquid exchange. a) Flow rates over time for equilibration solution (Q_{ES}), vitrification solution (Q_{VS}) sequentially dispensed ($Q > 0$) into hanging droplet (Video S3†). To keep a constant droplet volume whenever Q_{ES} or Q_{VS} flow, an equal amount of flow rate Q_W is aspirated ($Q < 0$) from hanging droplet into waste. Red and green bands respectively denote activation of pumps for ES and VS loading. b) Corresponding droplet volume over time during liquid exchange at Q = 2000 μL min^{-1} measured using real-time image analysis (Fig. S7† Materials and methods). c) Ratio of colors measured, where BS, ES and VS are respectively stained by blue, red and green color dye. d) Corresponding images of droplet during ES and VS loading. Numbers indicate time elapsed after starting each loading process.

characterizing liquid exchange for ES and VS loading; the color ratio curves eventually converge to a practically steady values (Fig. 4c and S6† red and green) that we used as a reference for estimating the time scale of liquid exchange.

Juxtaposing experiments with simulations, we compared the time scales of liquid exchange for ES and VS loading (Fig. 5 and S8†). Although extracting colors from a two-dimensional projected area (profile view) of the droplet can be prone to artifacts from imaging (Fig. S7†), the color characterization enabled us a tractable comparison between experiments and simulations. We calculated the time scale τ for liquid exchange as the time needed to reach 90% of steady-state value of color ratio for experiments (Fig. 4c and S8†) and mass ratio for simulations (Fig. 3c and f). Applying exponential or sigmoid fits on the collected data (Fig. 5, inset and S8†), we concluded that the time scales for liquid exchange are comparable for simulations and experiments, lying in the range of τ = 5–15 s (Fig. 5).

Vitrification of mouse eggs using programmable platform

We used the triple-step operation of our platform (Fig. 2) to vitrify eggs from a mouse cohort (Materials and methods). In accordance with manual vitrification protocols,[12] we programmed our platform to expose the eggs (n = 157) to ES for 10 min, followed by an exposure to VS for 1 min (Fig. 6a, b and Video S4†). Using our microscopy system (Fig. 2b, bottom and 6a) we monitored the morphology of the eggs during the entire operation of ES and VS loading (Fig. 7a and b). Imperfect focus in our egg images may temporarily introduce error in the measurement of cell size, thus we performed quantitative analysis to correlate error with degree of focus (Fig. S9†). With this analysis, we validated that our monitoring system can resolve the evolution of cell size during the vitrification protocol. We observed that upon ES loading, the eggs rapidly (within 10 s) start shrinking due to dehydration, reaching almost half of their pre-exposure

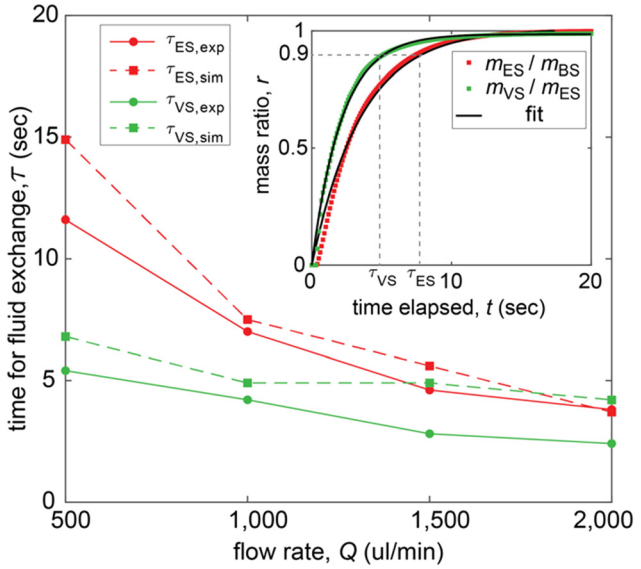

Fig. 5 Characterization of time for liquid exchange in hanging droplet. Comparison of time for liquid exchange for ES loading (red) and VS loading (green) between experiments (circles, continuous lines) and simulations (squares, dashed lines) at different flow rates. The time scale τ of liquid exchange is calculated as time needed to reach 90% of steady-state value (Fig. S8†) of respectively color ratio for experiments and mass ratio for simulations (inset shows simulation at Q = 1000 μL min^{-1}).

volume at around ~1 min. We expected this volume decrease due to the exposure to cryoprotectant components of ES, namely DMSO and ethylene glycol (EG) which cause dehydration of the egg.[40–43] Upon longer exposure to ES, the eggs start re-expanding due to the absorption of permeable cryoprotectants recovering half of the loss of pre-exposure volume at around ~10 min (Fig. 7a and b), a trend which is also consistent with previous studies.[42,43] Upon VS loading at 10 min, the eggs dramatically shrink to about half of their pre-exposure volume, which is a known phenomenon attributed to the effect of the sucrose to the egg.[42,43] Therefore, our observations of egg morphology, further validated that liquid exchange from BS to ES and finally to VS, indeed takes place in our platform. After VS loading, we unloaded the eggs from hanging droplet using Cryoloop (Fig. 2c and S4d†) and plunged them into liquid nitrogen for storage for a couple of days (Materials and methods).

To set a basis for comparison for evaluating the effectiveness of our automated platform, we also manually performed the ES, VS loadings and plunging processes using Petri dishes, pipettes and Cryoloop vitrification carriers, observing similar timings (Fig. 6c and d, Materials and methods). In the context of this study, we defined the post-vitrification survival as the metric of effectiveness. To robustly compare the automated and manual approach, we manually thawed all vitrified eggs and assessed their post-vitrification survival based on observation of their morphology by an expert embryologist using brightfield microscopy (Fig. S10 and S11†). Among the $n > 150$ eggs, we had similar recovery rates of the order of nearly 90% for both the automated and manual approaches (Fig. 7c, blue bars), as the post-thaw recovery was manually performed for all eggs. Regarding the post-thaw survival after vitrification, we observed comparable percentages (~95%) between the manual and automated approaches (Fig. 7c, red bars and S12†).

Discussion & conclusion

We have demonstrated a platform that yields post-vitrification egg survival that is comparable with that of a manual operator. Our platform features a disposable chip that we prototyped at low cost (tens of United States dollars per chip) and high speed (15 minutes per chip) *via* a simple fabrication process. Additionally, our platform enables a user-friendly interface with real-time egg monitoring capabilities, ensuring consistency in egg handling and customizable cryoprotectant loading. Particular to our design is the hanging droplet that offers a chamber for liquid exchange around the egg without contact with solid walls, minimizing the chances of physical damage while providing easy access for unloading the egg from the chip.

We envision that obtaining real-time images of the egg morphology may enable optimization of the vitrification process. Recent works have pointed to the dynamics of egg volume change during CPA loading as an argument for shortening the duration of the vitrification process.[42,44] These arguments are based on the hypothesis that it is not necessary to recover the rapid (occurring within 1 min) volume loss due to exposure to ES, thus suggest to skip the long (~10 min) equilibration process prior to exposure to VS. Notably, skipping the long equilibration process has recently yielded excellent post-vitrification results for human oocytes.[45] Using our advection-based CPA loading regime, our platform can realize thorough CPA exchange within seconds. This allows flexible and precise CPA concentration adjustment inside the hanging drop. As a result, our platform is adjustable to implement different CPA loading strategies, such as the gradual cryoprotectant loading that we have demonstrated in addition to rinsing modalities (Fig. S13 and Video S5†).

Compared with other egg freezing devices, our platform is compatible with existing vitrification carriers, which have proven performance in fertility clinics. Our hanging droplet chip allows egg unloading from the liquid–air interface using different vitrification carriers such as Cryotop and Cryoloop. While vitrification carriers such as the Capillary tube were more challenging to use in our system, Cryoloop was our preferred vitrification carrier as it minimizes the cryoprotectant volume around the egg after its unloading from the hanging droplet (Video S2†) without the need of additional pipetting steps to aspirate excess volume as in the case of Cryotop. However, eggs unloaded by Cryoloop can be subsequently transported to an open vitrification carrier (Cryotop) for long-term storage, and thawing (Video S6†).

There are several steps necessary for translating our platform to a clinical setting. First, a pilot study[46] focusing on post-vitrification fertilization of mouse eggs will follow-up

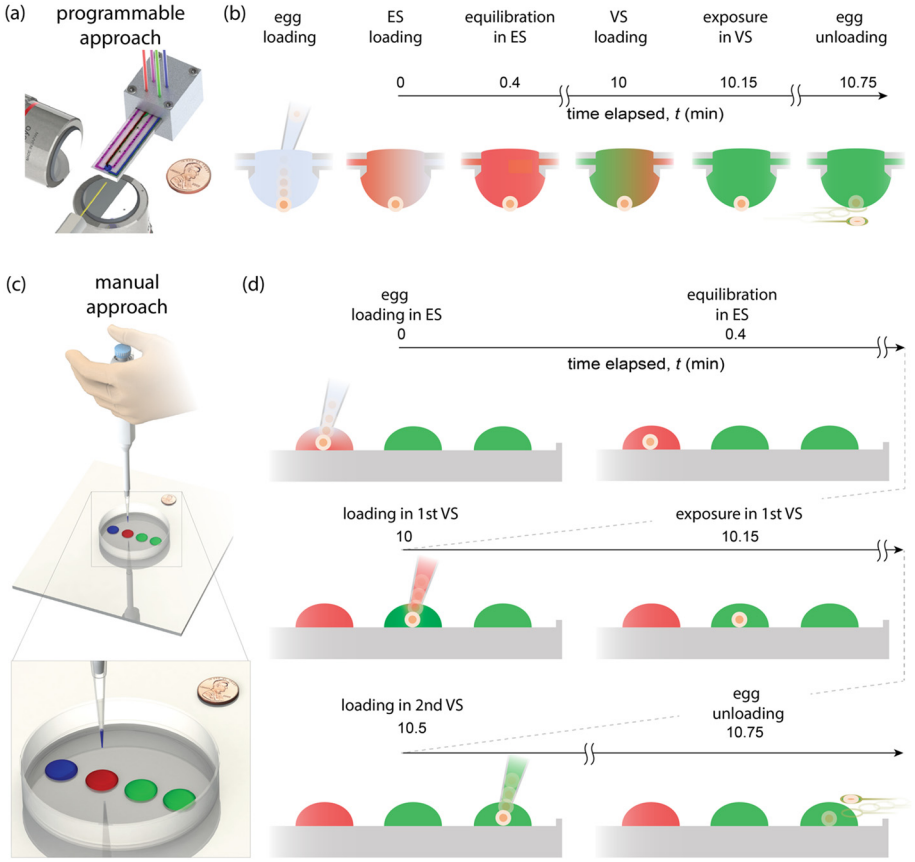

Fig. 6 Programmable and manual approach for vitrification of eggs. a) CAD file of microfluidic chip in full assembly, where a United States one-cent coin (diameter ~19 mm) denotes the scale. b) Recipe for performing exchange around the egg using our microfluidic set-up (Fig. 2), by sequentially flowing ES and VS solutions (Q_{ES} = 500 μL min^{-1}, Q_{VS} = 1500 μL min^{-1}) with a 10 min interval between the two for equilibration of the egg (Video S4†). c) CAD file of set-up for manual approach involving the use of hand-held micropipette and a Cryotop (orange) a vitrification carrier. d) Recipe for manually performing liquid exchange around the egg (first the egg stays in BS for 1 min which is not shown in panel d) by pipetting the egg in and out of standing droplets of 250 μL volume, including micromixing aspirations (not shown on schematic) leading to the unloading of the egg, using the cryoloop (bottom right), before eventually plunging it into liquid nitrogen.

this work, as the post-vitrification survival does not necessarily reflect preservation of reproductive potential.[40,41] Second, it will be necessary to improve the robustness of the device; despite its user-friendly characteristics, caution needs to be taken to de-risk remaining manual aspects of the device, such as egg loading (*i.e.* pipetting) and unloading (*i.e.* motorized vitrification carrier), that can still lead to egg loss or damage. For our experiments using the programmable platform, we observed that 15–20% of oocytes were lost during the unloading from the hanging droplet. Among vitrified cells, egg damage can be measured at the molecular level by examining the transcription profile of genes related to oxidative stress, endoplasmic reticulum stress, heat shock and apoptosis, which could all be affected by exposure to cryoprotectants.[30] In addition, several technical aspects, such as the removal of air bubbles in the system, need to be carefully addressed to ensure smooth implementation of the hanging droplet concept. In addition, the optical system can be upgraded using an autofocusing module for better monitoring of the eggs in real-time as well as by controlling the position of the objective *via* the motorized stage based on a software output of a focus metric. Using machine vision, our motorized system can be fully automated to detect and unload the egg.

Third, we believe that a clinical study with human donor eggs should account for regulatory aspects in advance, such as suitability of vitrification carrier,[47] compatibility with cryostorage systems,[48,49] contamination aspects (*e.g.* working solutions), environmental conditions, as well as the reproducibility and biocompatibility of disposable microfluidic devices, to mention just a few. Taken together, we believe that the implementation of our platform can be achieved by defining efficient workflows in the clinic, based on the interplay between the technology itself and human factors in the context of lab operations.[50]

Beyond assisted human reproduction, we envision that the potential of our platform extends to broader applications in cryopreservation from human stem cells,[51] laboratory animals and livestock[52] to equines[53] and biodiversity-related species.[54,55] Given the merits of our platform for programmable and monitorable vitrification, we envision that our device may bring a systematic approach to vitrification and help further advance its mechanistic understanding.

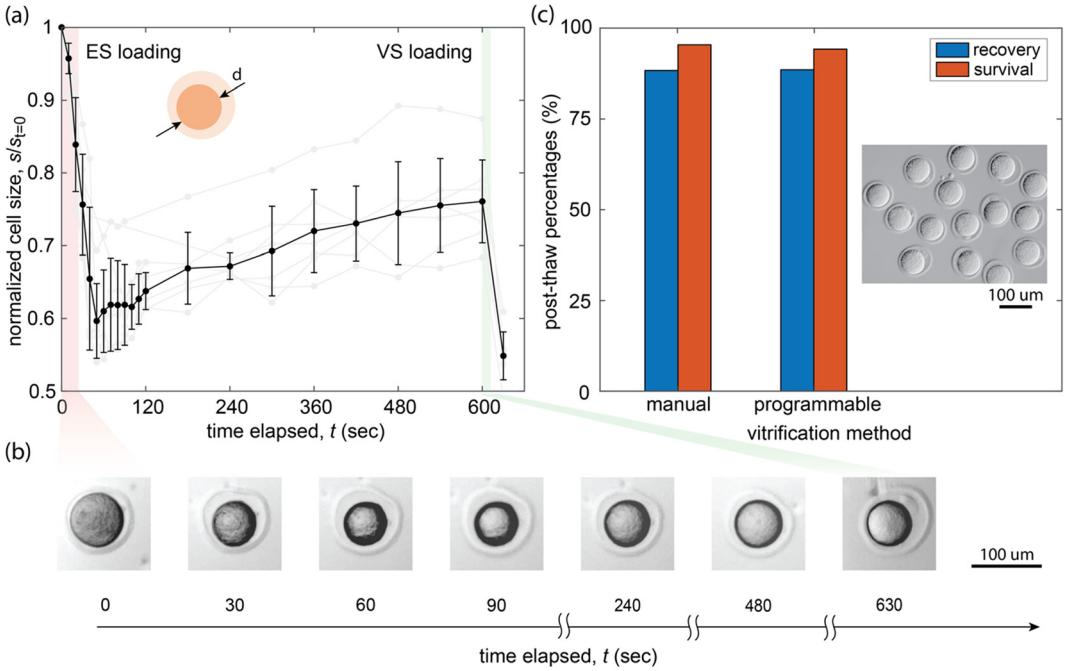

Fig. 7 Real-time observation of egg morphology during process of vitrification and process efficiencies. a) Diameter of egg, as average (black) of seven sample experiments (faint gray) as a function of time spanning ES and VS loading and equilibration in between. Time t = 0 denotes start of ES loading where egg is still in BS solution. Error bars denote standard deviation. Inset shows calculation of size (orange) inside of zona pellucida (cream) as $s \propto d^3$ where d is the cell diameter. b) Sample images of egg morphology during process of vitrification where background is removed and brightness adjusted. c) Post-vitrification percentages of recovery of eggs using Cryoloop (blue) and survival (red) of a cohort of $n > 150$ mouse eggs. The post-vitrification survival is comparable (~95%) between manual and automated method. The survival was determined based on phenotypical observation (Fig. S10–S12†). The inset shows a sample of eggs in media post-thaw after vitrification using automated approach.

Materials and methods

Chip fabrication

The microfluidic chip was fabricated through a thermal lamination process.[35] A co-extruded film composed of TOPAS 6015s04 (200 μm thickness) and TOPAS E140 (50 μm thickness) films was used.[34] With a semicrystalline and flexible structure, E140 has a low melting point (84 °C) and could be blended with other COC grades *via* thermal bonding. The multiple layer microfluidic channel and cover layers were plotted utilizing a vinyl cutter (GS2-24, Roland). Films get bonded together using a thermal laminator after rinsing and degassing (Fig. S1†). The rim structure, which extended hanging drop height and improves hanging drop stability, is manufactured utilizing a PCB milling machine (Bantam Tools Othermill V2). Then, E140 serves as the adhesive layer for the thermal bonding of the rim and open chamber chip. A cartridge was designed for the installation of microfluidic chip on the integrated system (Fig. 2b and S2†). The cartridge was made of acrylic or aluminum. It includes O-ring for chip sealing, port for tubing connection, and fixture to connect with integrated platform.

Cryoprotectant preparation and characterization

Cryoprotectants (CPAs) were prepared based on the reported protocols and verified through a toxicity test. The compositions of the CPAs are listed in Table 1. CPA fluid properties were characterized as they may affect CPA loading process and egg position. CPA viscosity was measured utilizing AR-G2 rheometer with a cone-plate geometry (TA Instrument, TX, USA). The surface tension was measured using a goniometer (Rame-Hart Model 590, NJ, USA). CPAs composition and measured properties are summarized in Table 1.

Mice and ovarian egg collection

Study procedures were performed under approval from the MIT Committee on Animal Care. Fourteen to twenty-week-old, superovulated, CD1-E mice (Taconic Biosciences, Germantown, NY, USA) were used for ovarian egg collection. Mice were maintained on normal, *ad libitum* rodent chow (LabDiet, Wayne County, IN, USA) and water. Mice were euthanized *via* cervical dislocation, followed by oviduct harvesting. Cumulus-egg complexes were incubated in FHM media (Millipore-Sigma, Burlington, MA) containing hyaluronidase (0.1%, Millipore-Sigma) for 2–3 minutes at room temperature to remove the eggs from the surrounding cumulus cells. The eggs were placed in HTF (Millipore-Sigma) medium supplemented with fetal bovine serum (FBS, 20%, Millipore-Sigma) for 15 minutes in an incubator supplemented with carbon dioxide (5%) and set at 37 °C.

Manual egg vitrification protocol

The performance of the automated egg freezing instrument is validated utilizing mouse eggs, and manual egg freezing

process is performed as comparison. During the manual egg freezing process, a 100 mm Petri dish was prepared with one drop of 250 μl BS, one drop of 250 μl ES, and 2 drops of 250 μl VS (Fig. 6c). Mouse eggs were incubated in the BS drop for 1 minute, then transfer to the ES drop for 10 minutes. After equilibration, mouse eggs were loaded into the first VS drop, stirring VS medium around the eggs using the pipette, and then the eggs were transferred into the second VS drop. The overall time between egg incubation in the first VS drop to the loading eggs on the Cryoloop and plunged into liquid nitrogen was 90 s (Fig. 6d).

The warming process was performed to evaluate the survival rates of eggs vitrified *via* manual or programmable methods. TS (4 mL) was prepared in a 35 mm Petri-dish that was warmed in an incubator for 2 hours before use. A Cryowand™ was used to transfer the Cryoloop out of the liquid nitrogen, and rapidly immerse the tip of Cryoloop into TS. Eggs were recovered from TS and transferred to DS after 60 s. After 3 minute treatment in DS, eggs were transferred into BS for 5 minutes for assessment egg condition and calculate the egg survival rate.

The previously vitrified eggs were observed after thawing using a brightfield microscope (Nikon Eclipse TE2000-S) utilizing 4× (Nikon 4X/0.10 WD 30) and 10× objectives (Modulation Optics Inc HMC 10X Plan/0.25). The digital images were taken using a SPOT Idea CMOS Microscope Camera on SPOT 5.6 software. The length scale for the images capturing the eggs was determined using a hemocytometer with minimum square area of grid 0.0025 mm^2 (Neubauer improved bright-line).

COMSOL modelling

COMSOL 6.1 was used for the simulation and evaluation of CPA loading process. The difference of fluid density and viscosity for BS, ES, and VS need to be considered, and we selected the transport of concentrated species (TCS) and laminar flow model to study the mixing of CPA components, in which BS, ES, and VS were classified as miscible species during simulation. Both the effects of advection and diffusion were considered in the simulation. Fick's law was used to characterize the diffusion across species, and the diffusion coefficient $D = 10^{-9}$ m s^{-1} is selected.[36] The hanging drop was described as a droplet with fixed volume, and the liquid–air interface was set to slip boundary condition.

Software

The integrated system (Fig. 2) was centrally controlled using LabVIEW 2020, 64 bit Professional Version including the NI Vision Development Module. The Arduino interfaced with LabVIEW using LINX – LabVIEW MakerHub. The motorized stages for both vertical objective and Cryoloop interfaced with LabVIEW using Thorlabs APT software. Post-processing of data was conducted using MATLAB 2019b, ImageJ 1.53q and Microsoft Excel 2019.

Optical system for programmable platform

Given the convex shape of the droplet, an illumination system providing non-collimated light into the droplet was designed. A cold-light Mounted LED (MCWHL5) was followed by a doublet-lens system (ACL2520U-A and ACL5040U-A, Thor Labs) for non-collimated light illumination into the chip holding the handing droplet. The immediately after the 4× objective (infinity-corrected, long working distance Nikon 4×, MRH00045), a right-angle kinematic mirror mount (KCB1, Thor Labs) was used, followed by a tube lens for widefield imaging (TTL200-A, Thor Labs) before the monochrome camera (Basler, a2A4504-18umPRO) for bottom view (Fig. 2b and S2†). No additional illumination system was used for side view. The length scale for the bottom view images capturing the eggs was determined using a resolution test target (Birefringent 1951 USAF Test Target, "3 × 1", Thorlabs, ReL1S1B).

Image analysis

The droplet volume was calculated in real-time (LabVIEW, NI Vision Development Module) using a brightness-thresholding algorithm (Fig. S7†). The algorithm recognized the droplet as a brighter object than the darker background. Given that the droplet focused the light as a convex lens due to its size (~20 μL), it exhibited a non-uniform brightness, in particular a bright tip extending to most of its profile, and a dark inner core (Fig. 1b side and 4d). To correctly capture the droplet, the edges of the rim were set, and the code connected the edges of the droplet's profile to the edges of the rim. Then, the droplet object was filled as a convex hull. Next, the profile and center axis of the droplet were extracted from the boundary of the object. Using the extracted profile, the droplet volume was calculated as a solid of revolution by integrating the radius of its profile around its center axis. Artifacts resulting from the real-time brightness-thresholding algorithm during ES and VS loading were eliminated by a post-processing algorithm implemented in MATLAB 2019b (Fig. S7†).

Data availability

The data that support the finding of this study is available in ESI.† For any additional requests or queries regarding the data, please contact Linda G Griffith at griff@mit.edu.

Author contributions

H. F., G. K., J. O. D., S. R. M., and L. G. G. conceived the study. H. F., G. K. and J. L., designed the study. H. F. and G. K. developed the experimental set-up, the automation software, conducted experiments, performed simulations, and analyzed data. I. D. N. and G. D. performed mouse surgeries, manual vitrification of oocytes and all thawing processes. S. R. M. and L. G. G. supervised the project. H. F. and G. K. wrote the manuscript. I. D. N., J. L, S. R. M. and L. G. G. provided comments on the manuscript.

Conflicts of interest

H. F., G. K., J. O. D., S. R. M., and L. G. G. are inventors of a patent application (PCT/US2024/012451) related to the technology discussed in this paper. J. O. D. and L. G. G. hold equity at Flash Inc. which develops technologies relevant to the research presented in this work.

Acknowledgements

The authors gratefully acknowledge the financial support from Massachusetts Life Sciences Center. We also thank Cryotech Inc and MIT Deshpande Center for Technological Innovation for their support and assistance that contributed to the initiation and completion of this research. Furthermore, H. F. thanks Prof. David Trumper from MIT for valuable discussions for problem definition and concept development. H. F. thanks Prof. Gareth McKinley from MIT for providing access to rheometer and goniometer instruments used for characterization of cryoprotectants used in this study. H. F and G. K. thank Maxine Jonas and Steve Wasserman from MIT for insightful discussions on the design of the optical system. G. K. thanks Alex Angelopoulos from Harvard Business School for fruitful discussions on trends and developments in the fertility space.

References

1 D. Whaley, K. Damyar, R. P. Witek, A. Mendoza, M. Alexander and J. R. T. Lakey, Cryopreservation: An Overview of Principles and Cell-Specific Considerations, *Cell Transplantation*, 2021, **30**, 1–12, DOI: **10.1177/0963689721999617** (acccessed 2024/04/11).

2 A. Q. Leung, K. Baker, D. Vaughan, J. S. Shah, A. Korkidakis, D. A. Ryley, D. Sakkas and T. L. Toth, Clinical outcomes and utilization from over a decade of planned oocyte cryopreservation, *Reproductive BioMedicine Online*, 2021, **43**(4), 671–679, DOI: **10.1016/j.rbmo.2021.06.024**.

3 Practice Committees of the American Society for Reproductive Medicine and the Society for Assisted Reproductive Technology, Mature oocyte cryopreservation: A guideline, *Fertility and Sterility*, 2013, **99**(1), 37–43, DOI: **10.1016/j.fertnstert.2012.09.028**.

4 Centers for Disease Control and Prevention, *2021 Assisted Reproductive Technology Fertility Clinic and National Summary Report*, US Dept of Health and Human Services, 2023.

5 J. O. Doyle, K. S. Richter, J. Lim, R. J. Stillman, J. R. Graham and M. J. Tucker, Successful elective and medically indicated oocyte vitrification and warming for autologous in vitro fertilization, with predicted birth probabilities for fertility preservation according to number of cryopreserved oocytes and age at retrieval, *Fertility and Sterility*, 2016, **105**(2), 459–466.e452, DOI: **10.1016/j.fertnstert.2015.10.026**.

6 F. Choucair, N. Younis and A. Hourani, The value of the modern embryologist to a successful IVF system: revisiting an age-old question, *Middle East Fertility Society Journal*, 2021, **26**(15), DOI: **10.1186/s43043-021-00061-8**.

7 Practice Committees of the American Society for Reproductive Medicine (ASRM) and the Society for Reproductive Biologists and Technologists (SRBT), Comprehensive guidance for human embryology, andrology, and endocrinology laboratories: management and operations: a committee opinion, *Fertility and Sterility*, 2022, **117**(6), 1183–1202, DOI: **10.1016/j.fertnstert.2022.02.016**.

8 A. Murphy, H. Baltimore, M. S. Lapczynski, G. Proctor Jr, E. C. Meyer, T. Glynn, A. D. Domar and M. G. Collins, Embryologist Burnout: Physical and Psychological Symptoms and Occupational Challenges Currently Reported By U S Embryologists, *Fertility and Sterility*, 2022, **118**(4), e66, DOI: **10.1016/j.fertnstert.2022.08.205**.

9 P. Mazur, Freezing of living cells: mechanisms and implications, *American Journal of Physiology-Cell Physiology*, 1984, **247**(3), C125–C142, DOI: **10.1152/ajpcell.1984.247.3.C125 (acccessed 2024/04/11)**.

10 A. Arav and Y. Natan, Vitrification of oocytes: From basic science to clinical application, *Adv. Exp. Med. Biol.*, 2013, **761**, 69–83, DOI: **10.1007/978-1-4614-8214-7_6**.

11 C. E. Argyle, J. C. Harper and M. C. Davies, Oocyte cryopreservation: where are we now?, *Human Reproduction Update*, 2016, **22**(4), 440–449, DOI: **10.1093/HUMUPD/DMW007**.

12 Z. P. Nagy, L. Nel-Themaat, C.-C. Chang, D. B. Shapiro and D. P. Berna, Cryopreservation of Eggs, in *Human Fertility: Methods and Protocols*, ed. Z. Rosenwaks and P. M. Wassarman, Springer, New York, 2014, pp. 439–454.

13 G. Vajta, P. Holm, M. Kuwayama, P. J. Booth, H. Jacobsen, T. Greve and H. Callesen, Open pulled straw (OPS) vitrification: A new way to reduce cryoinjuries of bovine ova and embryos, *Mol. Reprod. Dev.*, 1998, **51**(1), 53–58, DOI: **10.1002/(SICI)1098-2795(199809)51:1<53::AID-MRD6>3.0.CO;2-V**.

14 M. Kuwayama, G. Vajta, O. Kato and S. P. Leibo, Highly efficient vitrification method for cryopreservation of human oocytes, *Reproductive BioMedicine Online*, 2005, **11**(3), 300–308, DOI: **10.1016/S1472-6483(10)60837-1**.

15 R. Risco, H. Elmoazzen, M. Doughty, X. He and M. Toner, Thermal performance of quartz capillaries for vitrification, *Cryobiology*, 2007, **55**(3), 222–229, DOI: **10.1016/j.cryobiol.2007.08.006**.

16 N. N. Desai, J. M. Goldberg, C. Austin and T. Falcone, The new Rapid-i carrier is an effective system for human embryo vitrification at both the blastocyst and cleavage stage, *Reproductive Biology and Endocrinology*, 2013, **11**(1), 1–9, DOI: **10.1186/1477-7827-11-41**.

17 R. Samuel, H. Feng, A. Jafek, D. Despain, T. Jenkins and B. Gale, Microfluidic—based sperm sorting & analysis for treatment of male infertility, *Translational andrology and urology*, 2018, **7**(Suppl 3), S336–S347.

18 A. Karcz, A. Van Soom, K. Smits, R. Verplancke, S. Van Vlierberghe and J. Vanfleteren, Electrically-driven handling of gametes and embryos: taking a step towards the future of ARTs, *Lab Chip*, 2022, **22**(10), 1852–1875, DOI: **10.1039/d1lc01160j**.

19 H. Feng, A. Jafek, R. Samuel, J. Hotaling, T. G. Jenkins, K. I. Aston and B. K. Gale, High efficiency rare sperm separation from biopsy samples in an inertial focusing device, *Analyst*, 2021, **146**(10), 3368–3377, DOI: **10.1039/d1an00480h**.

20 A. Jafek, H. Feng, D. Broberg, B. Gale, R. Samuel, K. Aston and T. J. M. Jenkins, Nanofluidics, Optimization of Dean flow microfluidic chip for sperm preparation for intrauterine insemination, *Microfluid. Nanofluid.*, 2020, **24**, 1–9.

21 D. Lai, J. Ding, G. W. Smith, G. D. Smith and S. Takayama, Slow and steady cell shrinkage reduces osmotic stress in bovine and murine oocyte and zygote vitrification, *Hum. Reprod.*, 2015, **30**(1), 37–45, DOI: **10.1093/humrep/deu284**.

22 Y. S. Heo, H. J. Lee, B. A. Hassell, D. Irimia, T. L. Toth, H. Elmoazzen and M. Toner, Controlled loading of cryoprotectants (CPAs) to oocyte with linear and complex CPA profiles on a microfluidic platform, *Lab Chip*, 2011, **11**(20), 3530–3537, DOI: **10.1039/c1lc20377k**.

23 T. Scherr, S. Pursley, W. T. Monroe and K. Nandakumar, A numerical study on distributions during cryoprotectant loading caused by laminar flow in a microchannel, *Biomicrofluidics*, 2013, **7**(2), 24104, DOI: **10.1063/1.4793714**.

24 R. M. Zonis, *Development of an automated microfluidic system for the loading and unloading of cryoprotectants from mammalian oocytes*, Massachusetts Institute of Technology, Cambridge, 2020, **https://dspace.mit.edu/handle/1721.1/127111**.

25 Z. Lei, D. Xie, M. K. Mbogba, Z. Chen, C. Tian, L. Xu and G. Zhao, A microfluidic platform with cell-scale precise temperature control for simultaneous investigation of the osmotic responses of multiple oocytes, *Lab Chip*, 2019, **19**(11), 1929–1940, DOI: **10.1039/C9LC00107G, 10.1039/C9LC00107G**.

26 S. Miao, C. Guo, Z. Jiang, H. X. Wei, X. Jiang, J. Gu, Z. Hai, T. Wang and Y. H. Liu, Development of an Open Microfluidic Platform for Oocyte One-Stop Vitrification with Cryotop Method, *Biosensors*, 2022, **12**(9), 1–16, DOI: **10.3390/bios12090766**.

27 T. K. Roy, S. Brandi, N. M. Tappe, C. K. Bradley, E. Vom, C. Henderson, C. Lewis, K. Battista, B. Hobbs and S. Hobbs, *et al.* Embryo vitrification using a novel semi-automated closed system yields in vitro outcomes equivalent to the manual Cryotop method, *Hum. Reprod.*, 2014, **29**(11), 2431–2438, DOI: **10.1093/humrep/deu214**.

28 D. G. Pyne, J. Liu, M. Abdelgawad and Y. Sun, Digital microfluidic processing of mammalian embryos for vitrification, *PLoS One*, 2014, **9**(9), 1–7, DOI: **10.1371/journal.pone.0108128**.

29 B. Jiang, B. Huang, G. Cai, Y. Chen and T. Wu, Facile and highly efficient loading and freezing of cryoprotectants for oocyte vitrification based on planar microfluidics, *Microfluid. Nanofluid.*, 2021, **25**(8), 1–11, DOI: **10.1007/s10404-021-02462-7**.

30 P. Tirgar, F. Sarmadi, M. Najafi, P. Kazemi, S. Azizmohseni, S. Fayazi, G. Zandi, N. Ziaie, A. Shoushtari Zadeh Naseri, A. Ehrlicher and M. Dashtizad, *et al.*, Toward embryo cryopreservation-on-a-chip: A standalone microfluidic platform for gradual loading of cryoprotectants to minimize cryoinjuries, *Biomicrofluidics*, 2021, **15**(3), 034104, DOI: **10.1063/5.0047185**.

31 J. Barberet, B. Ducreux, C. Bruno, M. Guilleman, R. Simonot, N. Lieury, A. Guilloteau, D. Bourc'his and P. Fauque, Comparison of oocyte vitrification using a semi-automated or a manual closed system in human siblings: survival and transcriptomic analyses, *Journal of Ovarian Research*, 2022, **15**(1), 1–14, DOI: **10.1186/s13048-022-01064-3**.

32 J. Hajek, R. Baron, N. Sandi-Monroy, S. Schansker, B. Schoepper, M. Depenbusch, A. Schultze-Mosgau, K. Neumann, F. Gagsteiger, S. von Otte and G. Griesinger, A randomised, multi-center, open trial comparing a semi-automated closed vitrification system with a manual open system in women undergoing IVF, *Hum. Reprod.*, 2021, **36**(8), 2101–2110, DOI: **10.1093/humrep/deab140**.

33 T. Martín-Villalba, J. S. Fidalgo, P. Carasa, D. Garcia, C. D. Munuera, D. Cancio-Villalonga, S. Álvarez-Argüelles, G. Fernandez, E. Bajo and A. Fernandez, *et al.* Validation of an Oocyte Vitrification Using Davitri, a Novel Automated Microfluidics Device, *Fertility and Sterility*, 2021, **116**(3), e200–e201, DOI: **10.1016/j.fertnstert.2021.07.550**.

34 D. A. O'Boyle, *Integrated Disposable Microfluidic Tissue Chips*, Massachusetts Institute of Technology, Cambridge, 2021, **https://hdl.handle.net/1721.1/139362**.

35 H. Feng, M. Hockin, S. Zhang, M. Capecchi, B. Gale and H. Sant, Enhanced chromosome extraction from cells using a pinched flow microfluidic device, *Biomed. Microdevices*, 2020, **22**(2), 25, DOI: **10.1007/s10544-020-0477-7**.

36 H. C. Price, J. Mattsson and B. J. Murray, Sucrose diffusion in aqueous solution, *Phys. Chem. Chem. Phys.*, 2016, **18**(28), 19207–19216, DOI: **10.1039/c6cp03238a**.

37 T. Mukaida, S. Nakamura, T. Tomiyama, S. Wada, C. Oka, M. Kasai and K. Takahashi, Vitrification of human blastocysts using cryoloops: Clinical outcome of 223 cycles, *Hum. Reprod.*, 2003, **18**(2), 384–391, DOI: **10.1093/humrep/deg047**.

38 G. Saki and G. Dezfuly, Vitrification of human oocyte using cryoloop, *Iranian Journal of Reproductive Medicine*, 2005, **3**(1), 19–24.

39 X. Zhang, P. N. Catalano, U. A. Gurkan, I. Khimji and U. Demirci, Emerging technologies in medical applications of minimum volume vitrification, *Nanomedicine*, 2011, **6**(6), 1115–1129, DOI: **10.2217/nnm.11.71**.

40 A. Arav, Y. Natan, D. Kalo, A. Komsky-Elbaz, Z. Roth, P. E. Levi-Setti, M. Leong and P. Patrizio, A new, simple, automatic vitrification device: preliminary results with murine and bovine oocytes and embryos, *Journal of Assisted Reproduction and Genetics*, 2018, **35**(7), 1161–1161, DOI: **10.1007/S10815-018-1210-9**.

41 G. M. Fahy, Overview of biological vitrification, in *Vitrification in assisted reproduction*, ed. M. Tucker and J. Liebermann, CRC Press, 2016, p. 1.

42 M. Gallardo, J. Saenz and R. Risco, Human oocytes and zygotes are ready for ultra-fast vitrification after 2 minutes of exposure to standard CPA solutions, *Sci. Rep.*, 2019, **9**(1), 1–9, DOI: **10.1038/s41598-019-52014-x**.

43 A. Kader, A. Choi, R. K. Sharma, T. Falcone and A. Agarwal, Effect of varying equilibration time in a two-step vitrification method on the post-warming DNA integrity of mouse blastocysts, *Fertility and Sterility*, 2010, **93**(8), 2640–2645, DOI: **10.1016/j.fertnstert.2009.07.991**.

44 J. R. Cho, E. H. Yu, H. J. Lee, I. H. Kim, J. H. Jeong, D. B. Lee, S. K. Cho and J. K. Joo, Ultra-Fast Vitrification: Minimizing the Toxicity of Cryoprotective Agents and

Osmotic Stress in Mouse Oocyte Cryopreservation, *Int. J. Mol. Sci.*, 2024, **25**(3), 1884, DOI: **10.3390/ijms25031884**.

45 J. Liebermann, R. Brohammer, Y. Wagner, R. Smith, K. Even, J. Hirshfeld-Cytron and M. L. Uhler, Fast and furious: successful survival and resumption of meiosis in immature human oocytes vitrified and warmed in a short protocol, *Reproductive BioMedicine Online*, 2024, **49**(1), 103976–103976, DOI: **10.1016/j.rbmo.2024.103976**.

46 I. Napier, *Unpublished work regarding mouse egg IVF after vitrification*, 2024.

47 F. AbdelHafez, J. Xu, J. Goldberg and N. Desai, Vitrification in Open and Closed Carriers at Different Cell Stages: Assessment of Embryo Survival, Development, DNA Integrity and Stability during Vapor Phase Storage for Transport, *BMC Biotechnol.*, 2011, **11**(1), 29–29, DOI: **10.1186/1472-6750-11-29**.

48 S. Canosa, R. Maggiulli, D. Cimadomo, F. Innocenti, G. Fabozzi, G. Gennarelli, A. Revelli, F. Bongioanni, A. Vaiarelli and F. M. Ubaldi, *et al.* Cryostorage management of reproductive cells and tissues in ART: status, needs, opportunities and potential new challenges, *Reproductive BioMedicine Online*, 2023, **47**(3), 103252–103252, DOI: **10.1016/j.rbmo.2023.06.007**.

49 K. J. Go and C. Hudson, Deep technology for the optimization of cryostorage, *Journal of Assisted Reproduction and Genetics*, 2023, **40**(8), 1829–1834, DOI: **10.1007/s10815-023-02814-y**.

50 M. Alikani, K. J. Go, C. McCaffrey and D. H. McCulloh, Comprehensive evaluation of contemporary assisted reproduction technology laboratory operations to determine staffing levels that promote patient safety and quality care, *Fertility and Sterility*, 2014, **102**(5), 1350–1356, DOI: **10.1016/j.fertnstert.2014.07.1246**.

51 Y. H. Jeong, U. Kim, S. G. Lee, B. Ryu, J. Kim, A. Igor, J. S. Kim, C. R. Jung, J. H. Park and C. Y. Kim, Vitrification for cryopreservation of 2D and 3D stem cells culture using high concentration of cryoprotective agents, *BMC Biotechnol.*, 2020, **20**(1), 1–9, DOI: **10.1186/s12896-020-00636-9**.

52 M. Kamoshita, H. Sugita, A. Kageyama, Y. Kawata, J. Ito and N. Kashiwazaki, Recent advances of oocyte/embryo vitrification in mammals from rodents and large animals, *Animal Science Journal*, 2024, **95**(1), e13931, DOI: **10.1111/asj.13931** (accessed 2024/04/10).

53 N. Ortiz-Escribano, O. Bogado Pascottini, H. Woelders, L. Vandenberghe, C. De Schauwer, J. Govaere, E. Van den Abbeel, T. Vullers, C. Ververs and K. Roels, *et al.*, An improved vitrification protocol for equine immature oocytes, resulting in a first live foal, *Equine Veterinary Journal*, 2018, **50**(3), 391–397, DOI: **10.1111/evj.12747**.

54 R. L. Bolton, A. Mooney, M. T. Pettit, A. E. Bolton, L. Morgan, G. J. Drake, R. Appeltant, S. L. Walker, J. D. Gillis and C. Hvilsom, Resurrecting biodiversity: advanced assisted reproductive technologies and biobanking, *Reproduction and Fertility*, 2022, **3**(3), R121–R146, DOI: **10.1530/RAF-22-0005**.

55 S. Le Gac, M. Ferraz, B. Venzac and P. Comizzoli, Understanding and Assisting Reproduction in Wildlife Species Using Microfluidics, *Trends Biotechnol.*, 2021, **39**(6), 584–597, DOI: **10.1016/j.tibtech.2020.08.012**.